Title

Substitution of the D1-Asn87 site in photosystem II of cyanobacteria mimics the chloride-binding characteristics of spinach photosystem II

Journal

Journal of Biological Chemistry, 293(7)

ISSN

0021-9258

Authors

Banerjee, Gourab
Ghosh, Ipsita
Kim, Christopher J
et al.

Publication Date

2018-02-01

DOI

10.1074/jbc.m117.813170

Peer reviewed

Substitution of the D1-Asn^{87} site in photosystem II of cyanobacteria mimics the chloride-binding characteristics of spinach photosystem II

Received for publication, August 17, 2017, and in revised form, December 19, 2017 Published, Papers in Press, December 20, 2017, DOI 10.1074/jbc.M117.813170

Gourab Banerjee[‡1], **Ipsita Ghosh**[‡1], **Christopher J. Kim**[§], **Richard J. Debus**[§2], **and Gary W. Brudvig**[‡3]

From the [‡]*Department of Chemistry, Yale University, New Haven, Connecticut 06520-8107 and the* [§]*Department of Biochemistry, University of California, Riverside, California 92521*

Edited by Joseph M. Jez

Photoinduced water oxidation at the O_2-evolving complex (OEC) of photosystem II (PSII) is a complex process involving a tetramanganese-calcium cluster that is surrounded by a hydrogen-bonded network of water molecules, chloride ions, and amino acid residues. Although the structure of the OEC has remained conserved over eons of evolution, significant differences in the chloride-binding characteristics exist between cyanobacteria and higher plants. An analysis of amino acid residues in and around the OEC has identified residue 87 in the D1 subunit as the only significant difference between PSII in cyanobacteria and higher plants. We substituted the D1-Asn^{87} residue in the cyanobacterium *Synechocystis* sp. PCC 6803 (wildtype) with alanine, present in higher plants, or with aspartic acid. We studied PSII core complexes purified from D1-N87A and D1-N87D variant strains to probe the function of the D1-Asn^{87} residue in the water-oxidation mechanism. EPR spectra of the S_2 state and flash-induced FTIR spectra of both D1-N87A and D1-N87D PSII core complexes exhibited characteristics similar to those of wildtype *Synechocystis* PSII core complexes. However, flash-induced O_2-evolution studies revealed a decreased cycling efficiency of the D1-N87D variant, whereas the cycling efficiency of the D1-N87A PSII variant was similar to that of wildtype PSII. Steady-state O_2-evolution activity assays revealed that substitution of the D1 residue at position 87 with alanine perturbs the chloride-binding site in the proton-exit channel. These findings provide new insight into the role of the D1-Asn^{87} site in the water-oxidation mechanism and explain the difference in the chloride-binding properties of cyanobacterial and higher-plant PSII.

This work was supported by grants from the Department of Energy, Office of Basic Energy Sciences, Division of Chemical Sciences. Oxygen-release and EPR studies were supported by Grant DE-FG02-05ER15646 (to G. W. B.). Mutant construction, whole cell fluorescence measurements, and FTIR studies were supported by Grant DE-SC0005291 (to R. J. D.). The authors declare that they have no conflicts of interest with the contents of this article.

This article contains Table S1, Figs. S1–S10, supplemental Methods, and Notes S1 and S2.

[1] Both authors contributed equally to this work.

[2] To whom correspondence may be addressed. Tel.: 951-827-3483; Fax: 951-827-4294; E-mail: richard.debus@ucr.edu.

[3] To whom correspondence may be addressed. Tel.: 203-432-5202; Fax: 203-432-6144; E-mail: gary.brudvig@yale.edu.

Photosystem II (PSII)[4] is a 700-kDa pigment–protein complex responsible for water oxidation in photoautotrophic organisms. The site of water oxidation, known as the oxygen-evolving complex (OEC), consists of a μ-oxo-bridged tetramanganese-calcium cluster ligated by a number of amino acid residues and water molecules (1). The OEC is surrounded by a network of hydrogen-bonded amino acid residues and water molecules that, along with Cl^- ions, play a pivotal role in water oxidation (2, 3). This process is initiated by photoinduced charge separation via a chlorophyll molecule called P_{680}. The $P_{680}^{\bullet+}$ species thus formed is reduced by oxidation of the tetramanganese cluster, thereby building up oxidizing equivalents that are used for water oxidation (4). The process of water oxidation has been shown to proceed via a four-flash cycle called the Kok cycle with the intermediates formed at each step being referred to as S_i states (where $i = 0-4$) (5). The transient S_4 state has remained elusive so far, whereas the remaining S states have been studied using many experimental methods, especially EPR, FTIR, and extended X-ray absorption fine structure spectroscopy. Information about the S_0–S_3 states provides valuable insights about water oxidation.

Because of the ease of generation and detection of the S_2 state during S-state cycling, this state has been studied extensively. EPR studies of the S_2 state in PSII from spinach reveal two distinct spin isomers corresponding to $S = 1/2$ ($g = 2$) and $S = 5/2$ ($g = 4.1$) states that exist in equilibrium with each other (6–8). In cyanobacterial PSII, however, the S_2-state EPR spectrum exhibits only the $S = 1/2$ spin isomer (8). This indicates that even though the core of the OEC is highly conserved, there are differences in the surrounding hydrogen-bonding network that affect the equilibrium between these two spin isomers. Because the fundamental process of water oxidation is assumed to remain unchanged over evolution, analyzing the basis and importance of the surrounding amino acid residues is key to understanding the mechanism of water oxidation in greater depth. Previous studies have shown that the equilibrium between the two S_2-state isomers can be affected by a number of different factors such as temperature and small molecules like acetate, fluoride, and nitrite (8, 9). All of these factors affect the hydrogen-bonding network surrounding the OEC, thereby

[4] The abbreviations used are: PSII, photosystem II; Chl, chlorophyll; D1, D1 polypeptide of PSII; D2, D2 polypeptide of PSII; OEC, oxygen-evolving complex.

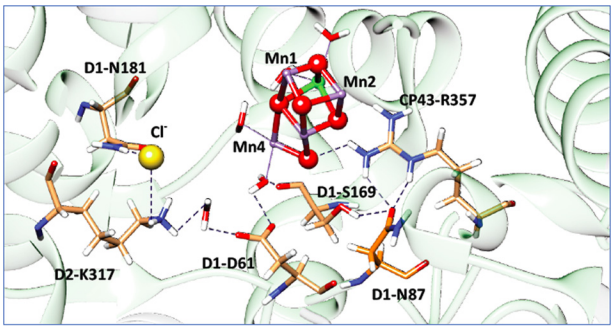

Figure 1. Structure of the OEC depicting the hydrogen-bonding network connecting D1-Asn^{87}, D1-Asp^{61}, and Cl$^-$ (Cl$^-$ marked in *yellow*) in cyanobacterial PSII.

stabilizing one of the two isomers. Also, it has been observed that depletion of Cl^- favors the $S = 5/2$ spin isomer in the S_2 state of spinach PSII (10, 11). This observation, however, has not been seen in cyanobacterial PSII indicating that the Cl^--binding site and its associated hydrogen-bonding network affects the spin isomer distribution differently in the two species (12). Mutations of second-shell residues in cyanobacterial PSII such as D2-K317R, D1-N181A, and D1-N181S have yielded the high-spin, S = 5/2, form of the S_2 state, highlighting the importance of these residues in the spin isomer equilibrium distribution (3, 13). Therefore, it is of interest to focus on changes in the second-shell residues that may impact the hydrogen-bonding network.

Sequence alignment studies of the second-shell residues have revealed that the only statistically significant difference between the two species occurs at D1 position 87 (2). This site is occupied by an asparagine residue in a significant majority of cyanobacterial PSII including *Synechocystis* PCC 6803 as opposed to an alanine residue in spinach PSII. Furthermore, this residue is an important part of the "narrow" channel of hydrogen-bonded waters whose role is yet to be determined (2). The hydrogen-bonding network surrounding the manganese cluster is extensive; therefore, perturbation at any point might be propagated over a long distance and can affect remote sites like the Cl^--binding site which is ~13 Å from D1 residue 87. Fig. 1 shows the extensive hydrogen-bonding network connected to D1 residue 87 in cyanobacterial PSII obtained from *Thermosynechococcus elongatus* (Protein Data Bank code 3WU2). Based on these observations it is therefore hypothesized that substitution of D1 residue 87 in cyanobacterial PSII would be able to effect some of the changes that are different in the two species. The current study deals with characterization of substitutions of D1 residue 87, specifically D1-N87A and D1-N87D. In addition to understanding the role of this site, our study also has uncovered some of the fundamental aspects that are different between the two species and hence provides new insight into the mechanism of water oxidation.

Results

Growth and steady-state oxygen assay

To investigate the significance of the difference in D1 residue 87 between spinach PSII and cyanobacterial PSII, the D1-N87A and D1-N87D mutations were constructed in *Synechocystis* sp. PCC 6803. D1-N87A cells and D1-N87D cells exhibit photoautotrophic growth. The doubling times of D1-N87A and D1-N87D cells were 26 and 21 h, respectively, compared with 14 h for wildtype cells (Fig. S1). The light-saturated O_2-evolution rates of D1-N87A and D1-N87D cells were 64 ± 4 and 36 ± 2% compared with the rate of wildtype cells, respectively (Table S1 and Note S1). On the basis of the maximum fluorescence yields ($F_{max} - F_0$) of wildtype, D1-N87A, and D1-N87D cells, the PSII contents of D1-N87A and D1-N87D cells were estimated to be 73 ± 5 and 36 ± 4% compared with wildtype cells, respectively (Fig. S2, Table S1, and Note S1). On the basis of measurements of the kinetics of charge recombination between $Q_A^{\cdot-}$ and the donor side of PSII following 5 s of actinic illumination in the presence of 3-(3,4-dichlorophenyl)-1,1-dimethylurea (DCMU), it was estimated that 10–14% of PSII reaction centers in D1-N87A and D1-N87D cells lack Mn_4CaO_5 clusters *in vivo* (Fig. S3 and Note S2). The presence of PSII reaction centers lacking Mn_4CaO_5 clusters implies that the Mn_4CaO_5 cluster is assembled less efficiently or is less stable in D1-N87A and D1-N87D cells compared with wildtype.

Table 1
Effect of Cl^- on O_2-evolution activity
Each value represents an average of three or more samples. Assays were carried out as described under "Experimental procedures."

Sample	PSII activity	
	+ 60 mM Cl^-	+ 0.1 mM Cl^-
	μmol of O_2 (mg of chl)$^{-1}$ h^{-1}	
Synechocystis (wildtype) PSII core complexes	3400 ± 83	2992 ± 35
D1-N87A PSII core complexes	3100 ± 56	1360 ± 46
D1-N87D PSII core complexes	886 ± 28	744 ± 15
Spinach PSII membranes	650 ± 35	286 ± 29

The light-saturated rates of O_2 evolution in PSII core complexes isolated from D1-N87D and D1-N87A cells were 886 ± 28 and 3100 ± 56 μmol of O_2 (mg of Chl)$^{-1}$ h^{-1}, respectively, compared with 3400 ± 83 μmol of O_2 (mg of Chl)$^{-1}$ h^{-1} for wildtype PSII core complexes under similar assay conditions using a buffer containing 60 mM Cl^- (Table 1). The lower PSII activity in the D1-N87D core complex can be due to inefficient assembly of the OEC, impaired S-state cycling or due to inactivation during biochemical isolation of PSII core complexes.

Cl^- dependence of steady-state oxygen evolution

To study the effect of Cl^- on the steady-state oxygen evolution of D1-N87A and D1-N87D PSII, the PSII core complexes were suspended in a buffer containing 0.1 mM Cl^-. The light-saturated activity of D1-N87D and D1-N87A PSII under this condition is given in Table 1. Under low Cl^- conditions, the oxygen-evolution activity of D1-N87D PSII decreased by 16% relative to Cl^--sufficient conditions. The Cl^- dependence of D1-N87D PSII is comparable with that of wildtype *Synechocystis* PSII core complexes, which exhibit a decrease in activity of only 12% under similar experimental conditions. However, the Cl^- dependence of D1-N87A PSII is markedly different from wildtype *Synechocystis* PSII, with a 56% decrease in the oxygen-evolution activity in low Cl^- conditions relative to Cl^--sufficient conditions; notably, this decrease is comparable with the 52% decrease observed for spinach PSII membranes (Table 1). These results demonstrate that the D1-N87A mutation modulates the Cl^--binding site, causing the Cl^- dependence of PSII

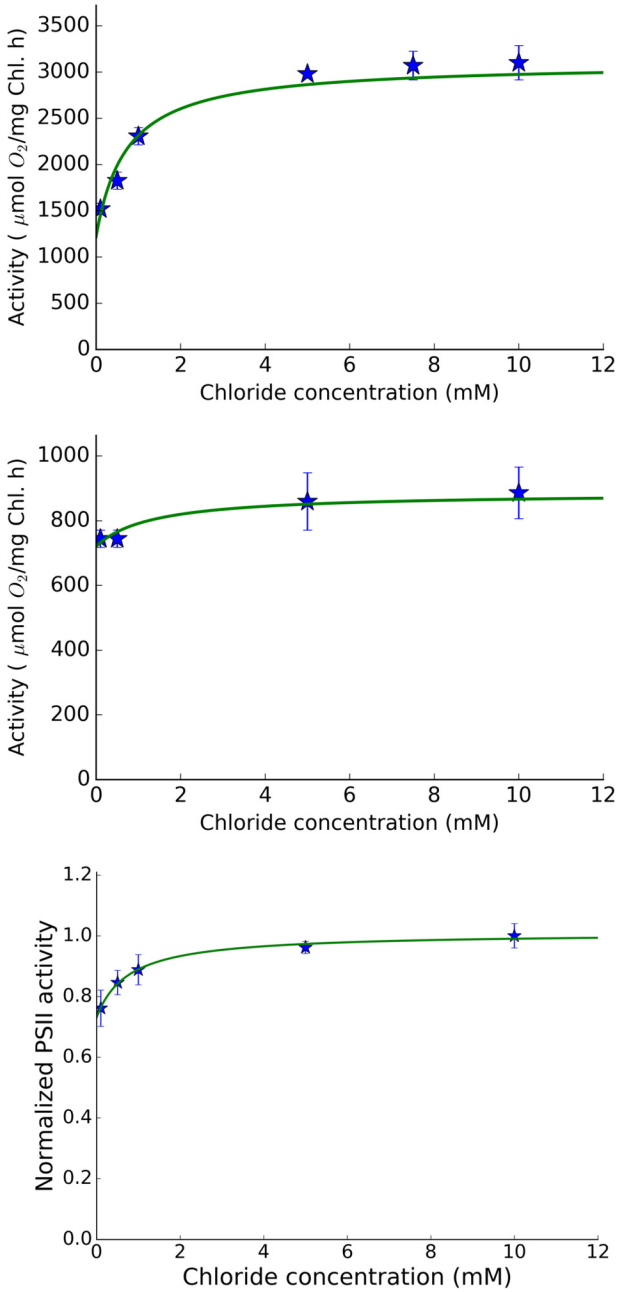

Figure 2. Effect of Cl^- on O_2-evolution activity of PSII core complexes isolated from: D1-N87A–mutated cells (*top panel*), D1-N87D–mutated cells (*middle panel*), and wildtype cells (*bottom panel*). Assays were carried out as described under "Experimental procedures." The data points were fit to a biphasic Michaelis–Menten equation (Equation 1).

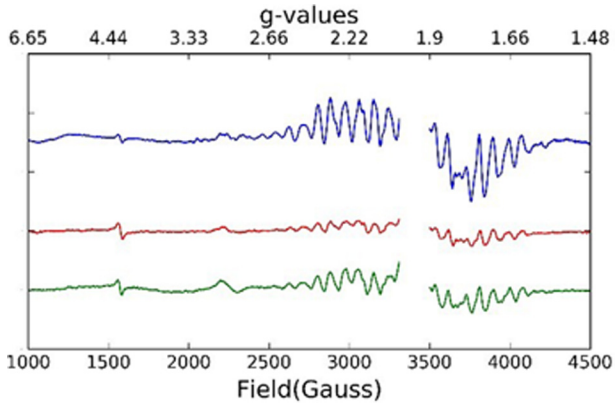

Figure 3. S_2-*minus*-S_1 difference EPR spectra of *Synechocystis* PSII core complexes: wildtype (*blue*), D1-N87D (*red*), and D1-N87A (*green*). The PSII activities (in μmol of O_2 (mg of Chl)$^{-1}$ h^{-1}) of the EPR samples are as follows: 2461 ± 49 (wildtype), 1255 ± 74 (D1-N87A), and 738 ± 38 (D1-N87D).

activity to be similar to spinach PSII. It is interesting, however, that the D1-N87D substitution has little effect on Cl^- binding.

Based on these results, we investigated the effect of these single-point mutations at D1 residue 87 on the binding affinity of chloride. The Cl^- concentrations were varied from 0.1 to 5 mM, and their effect on PSII activity was measured. The observation of biphasic binding curves (Fig. 2) suggests the presence of at least two types of Cl^--binding sites: one in which the bound chloride is exchangeable with free chloride (which titrates with a binding constant of K_D) and another non-exchangeable site (which gives activity in the absence of added chloride). The binding curves were computed by fitting the data to a biphasic Michaelis–Menten equation (Equation 1),

$$V_{obs} = f \times V_{max} + \frac{(1-f) \times V_{max} \times [Cl^-]}{K_D + [Cl^-]} \quad \text{(Eq. 1)}$$

where V_{obs} is the observed rate of oxygen evolution, V_{max} is the maximum observed activity which is normalized to 1, f is the fraction of centers with non-exchangeable Cl^-, and K_D is the binding constant of the exchangeable Cl^-. The measured K_D values for Cl^- in D1-N87A and D1-N87D PSII are 0.730 ± 0.218 mM (f = 0.4) and 1.35 ± 0.956 mM (f = 0.8), respectively, which fall within the range of K_D values obtained for Cl^- in spinach PSII (0.5–0.7 mM) (14–16). These results indicate that the binding environment of the exchangeable Cl^- in the two D1-Asn^{87}–substituted PSII samples is similar to that in spinach PSII. However, the fraction of exchangeable Cl^- is much larger in D1-N87A *Synechocystis* PSII and spinach PSII than in wildtype *Synechocystis* PSII and D1-N87D *Synechocystis* PSII.

Electron paramagnetic resonance spectroscopy

EPR experiments recording the S_1- and S_2-state spectra of spinach PSII membranes, and *Synechocystis* wildtype, D1-N87A and D1-N87D PSII core complexes were performed (S_2-*minus*-S_1 difference spectra shown in Fig. 3, unsubtracted spectra are included in Fig. S4, EPR spectra of spinach PSII membranes are included in Fig. S9). EPR spectra of D1-N87A were also collected after changing the cryoprotectant to sucrose. The spectrum in the presence of sucrose is similar to the spectrum in 10% (v/v) glycerol as cyoprotectant (Fig. S10). The dark spectra corresponding to the S_1 state exhibit a cytochrome c_{550} signal. Upon 200 K illumination, the OEC advances to the S_2 state, which is characterized by the presence of a g = 2 multiline EPR signal. The multiline signal was observed in wildtype, D1-N87A, and D1-N87D PSII (Fig. 3). However, the S = 5/2 spin isomer giving the S_2-state g = 4.1 signal that is observed under these conditions in spinach PSII membranes was absent in both D1-N87D and D1-N87A PSII. In addition, the S_2-*minus*-S_1 difference spectra show a light-induced cytochrome b_{559} signal at g = 3. The fraction of PSII

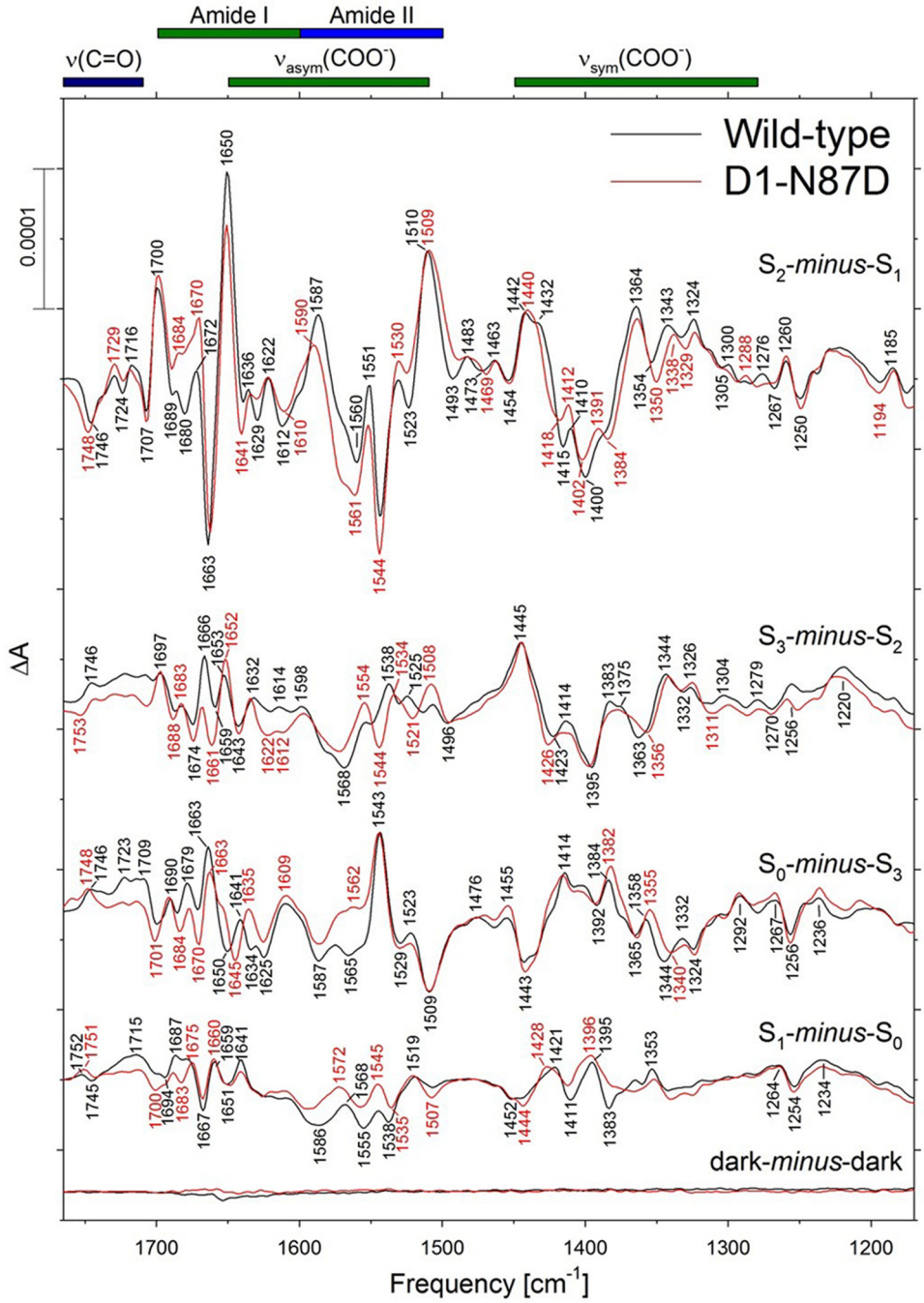

Figure 4. Comparison of the mid-frequency FTIR difference spectra of wildtype (*black*) and D1-N87D (*red*) *Synechocystis* PSII core complexes in response to four successive flash illuminations applied at 0 °C. The data (plotted from 1770 cm^{-1} to 1170 cm^{-1}) represent the averages of 12 wildtype and 17 D1-N87D samples (18,000 and 25,500 scans, respectively). To facilitate comparisons, the individual spectra of the D1-N87D samples were multiplied vertically by factors of 1.4, 1.1, 1.9, and 1.3, respectively, after normalization to the average absolute amplitudes of the samples at the amide I peak at 1657 cm^{-1}. Dark-*minus*-dark control traces are included to show the noise level (*lower traces*).

centers lacking a functional OEC gives rise to this signal when the sample is illuminated at 200 K. The intensities of $g = 2$ multiline signal of D1-N87D and D1-N87A PSII are smaller relative to wildtype PSII for a similar chlorophyll concentration. Both the weaker $g = 2$ multiline signal and the 200 K light-induced cytochrome b_{559} signal indicate that the D1-N87D and D1-N87A PSII samples have fewer functional OECs, consistent with the lower oxygen-evolution activity observed for the EPR samples.

FTIR spectroscopy mid-frequency region

The mid-frequency FTIR difference spectra induced by four successive flashes given to wildtype and D1-N87D PSII core complexes are compared in Fig. 4 (*black* and *red traces*, respectively). The spectra that are induced by the first, second, third, and fourth flashes correspond predominantly to the S$_2$-*minus*-S$_1$, S$_3$-*minus*-S$_2$, S$_0$-*minus*-S$_3$, and S$_1$-*minus*-S$_0$ FTIR difference spectra, respectively (17–20).

The mid-frequency S_2-*minus*-S_1 spectrum of D1-N87D PSII core complexes showed substantial changes compared with wildtype PSII throughout the mid-frequency region (*upper red trace* in Fig. 4). In the carbonyl stretching [ν(C=O)] region, the negative feature at 1746 cm^{-1} was broadened slightly and shifted ~2 cm^{-1} to higher frequency. In the amide I region, the negative features at 1689 and 1680 cm^{-1} were replaced by positive features at 1684 and 1670 cm^{-1}, and the negative feature at 1629 cm^{-1} was replaced by a negative feature at 1641 cm^{-1}. These features correspond to amide I modes because they shift significantly to lower frequencies after global incorporation of ^{13}C (21, 22) but not appreciably after global incorporation of ^{15}N (21, 22). In the overlapping asymmetric carboxylate stretching [$\nu_{asym}(COO^-)$]/amide II region, the positive feature at 1586 cm^{-1} was shifted ~3 cm^{-1} to higher frequency and diminished in amplitude, the 1560(−), 1551(+), and 1544(−) cm^{-1} features shifted downward, and the 1523(−) cm^{-1} feature was diminished. The 1587 cm^{-1} feature corresponds to a $\nu_{asym}(COO^-)$ mode because it shifts 30–35 cm^{-1} to lower frequency after global incorporation of ^{13}C (21–24) but is largely insensitive to the global incorporation of ^{15}N (3, 21–23, 25). The 1560(−), 1551(+), and 1544(−) features correspond to amide II modes because they shift appreciably to lower frequencies after global incorporation of either ^{13}C (21–24) or ^{15}N (3, 21–23, 25). In the symmetric carboxylate stretching [$\nu_{sym}(COO^-)$] region, the positive shoulder at 1432 cm^{-1} was eliminated; features at 1415(−), 1410(+), and 1400(−) cm^{-1} were shifted ~2 cm^{-1} to higher frequencies; features at 1354(−) and 1343(+) cm^{-1} were shifted 4–5 cm^{-1} to lower frequencies; and a negative feature at 1384 cm^{-1} appeared.

The mid-frequency S_2-*minus*-S_1 spectrum of D1-N87A PSII core complexes (Fig. S6, *upper red trace*) showed changes similar to those observed for D1-N87D PSII core complexes. The mid-frequency S_3-*minus*-S_2, S_0-*minus*-S_3, and S_1-*minus*-S_0 difference spectra of D1-N87D PSII core complexes (Fig. 4, *middle three pairs of spectra*) showed changes in the amide I and overlapping $\nu_{asym}(COO^-)$/amide II regions but fewer changes in $\nu_{sym}(COO^-)$ regions than in the S_2-*minus*-S_1 spectrum. In the S_3-*minus*-S_2 spectrum, the positive feature at 1746 cm^{-1} shifted to 1743 cm^{-1}, the positive feature at 1666 cm^{-1} was eliminated, a negative feature at 1651 cm^{-1} appeared, the amplitudes of negative features near 1622 and 1612 cm^{-1} increased, the amplitude of the negative feature at 1568 cm^{-1} decreased, new derivative-shaped features appeared at 1554(+)/1544(−) and 1546(−)/1506(+) cm^{-1}, and the negative feature at 1363 cm^{-1} shifted to 1356 cm^{-1} and decreased in amplitude. In the S_0-*minus*-S_3 spectrum, the positive feature at 1746 cm^{-1} shifted to 1748 cm^{-1}, the positive features at 1723 and 1709 cm^{-1} were eliminated, the derivative-shaped feature at 1650(−)/1641(+) cm^{-1} shifted to 1645(−)/1635(+) cm^{-1}, the negative feature at 1565 cm^{-1} was eliminated, and the derivative-shaped feature at 1358(+)/1344(−) cm^{-1} shifted to 1355(+)/1340(−) cm^{-1}. In the S_1-*minus*-S_0 spectrum, the derivative-shaped feature at 1753(+)/1745(−) cm^{-1} shifted to 1751(+)/1743(−) cm^{-1}, the positive feature at 1715 cm^{-1} was replaced by a negative feature at 1700 cm^{-1}, the positive feature at 1687 cm^{-1} was replaced by a negative feature at 1683 cm^{-1}, the negative feature at 1586 cm^{-1} was eliminated, the positive feature at 1568 cm^{-1} was shifted to 1572 cm^{-1}, a negative feature appeared at 1507 cm^{-1}, the positive feature at 1421 cm^{-1} shifted to 1428 cm^{-1}, and the negative feature at 1383 cm^{-1} was eliminated. The mid-frequency S_3-*minus*-S_2, S_0-*minus*-S_3, and S_1-*minus*-S_0 difference spectra of D1-N87A PSII core complexes (Fig. S6, *middle three pairs of spectra*) showed changes similar to those observed for D1-N87D PSII core complexes.

Strongly H-bonded O–H stretching region

The O–H stretching vibrations of strongly H-bonded OH groups can be observed as very broad positive features between 3200 and 2500 cm^{-1} (13, 26–29). These regions of the S_n-*minus*-S_{n+1} difference spectra of D1-N87D PSII core complexes are compared with wildtype PSII core complexes in Fig. 5. In the S_2-*minus*-S_1 spectrum (Fig. 5, *upper left panel*), the broad feature is overlain with numerous positive features that have been attributed to a mixture of C-H stretching vibrations from aliphatic groups and N-H stretching vibrations and their Fermi resonance overtones from the imidazole group(s) of one or more histidine residues (29–31).

The D1-N87D mutation caused no substantial alterations to the broad features of any of the S_n-*minus*-S_{n+1} spectra. The same is true for the D1-N87A mutation (Fig. S7).

Weakly hydrogen-bonded O–H and O–D stretching regions

The O–H stretching vibrations of weakly hydrogen-bonded OH groups of water molecules can be observed between 3700 and 3500 cm^{-1} (13, 26, 27, 29, 30, 32–41). The D1-N87D mutation eliminated the positive feature at 3619 cm^{-1} and shifted the negative feature at 3584 cm^{-1} feature to 3586 cm^{-1} in the in the S_2-*minus*-S_1 spectrum (Fig. 6, *upper left panel*), slightly diminished the amplitude of the broad feature centered at 3600 cm^{-1} in the S_3-*minus*-S_2 spectrum (Fig. 6, *lower left panel*), but had no apparent effect on the broad features centered at 3620 and 3610 cm^{-1} in the S_0-*minus*-S_3 and S_1-*minus*-S_0 spectra, respectively (Fig. 6, *upper* and *lower right panels*, respectively). Changes produced by the D1-N87A mutation (Fig. S8) resembled those produced by the D1-N87D mutation.

Polarographic O_2 measurements

To probe the S-state cycling, flash induced polarographic O_2-yield measurements were taken for PSII core complexes isolated from His-tagged wildtype, D1-N87A, and D1-N87D strains. The O_2-yield patterns are shown in Fig. 7.

The high intensity of the signal corresponding to the first flash in D1-N87D–mutated PSII may be attributed to the presence of damaged centers. The four-periodic oscillation pattern was fit to a modified Kok model (42). The miss and double-hit factors thereby computed are reported in Table 2. The miss factor for D1-N87A PSII core complexes is 11%, and that for D1-N87D core complexes is 29% compared with 14% for His-tagged wildtype PSII core complexes and 10% for spinach PSII (43). The percentage of double hits was small and did not vary significantly among the three types of PSII core-complexes. The oxygen-release kinetics for D1-N87D PSII core complexes was found to be similar to that of His-tagged wildtype PSII core complexes (Fig. S5).

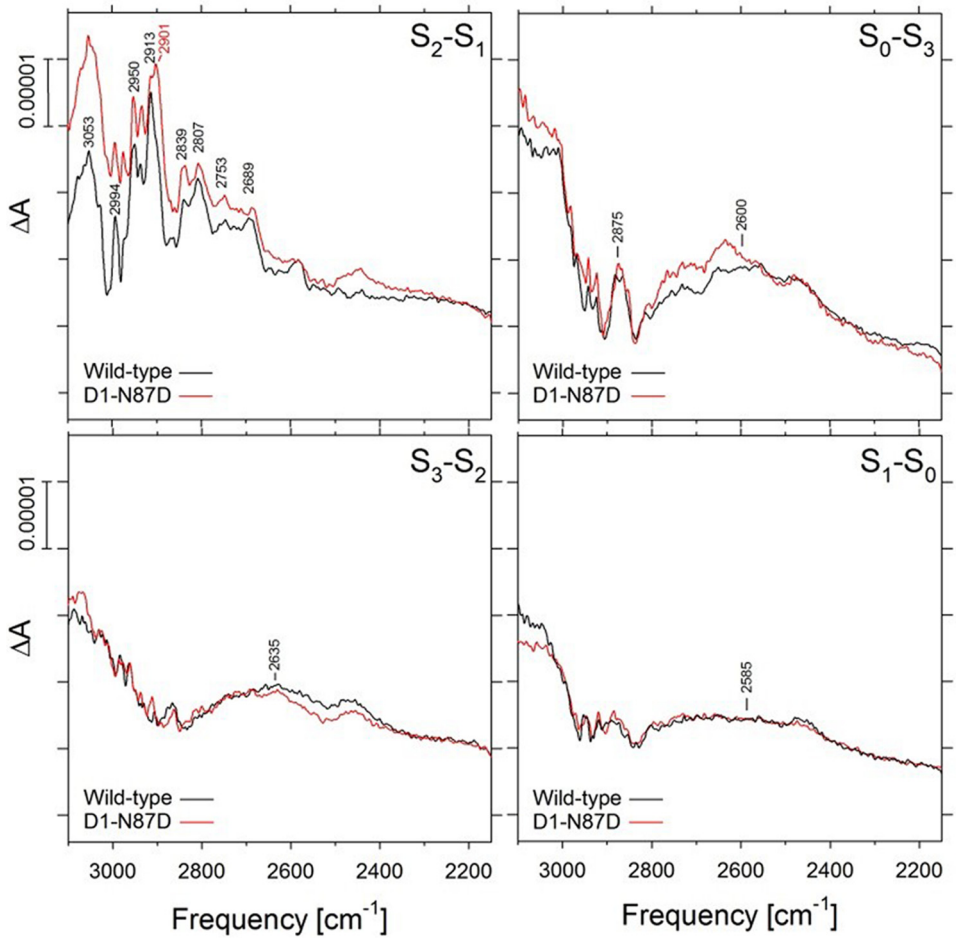

Figure 5. Comparison of the FTIR difference spectra of wildtype (*black*) and D1-N87D (*red*) *Synechocystis* PSII core complexes between 3100 and 2150 cm^{-1} in response to four successive flash illuminations applied at 0 °C. The data were collected simultaneously with that shown in Fig. 4. The *spectra* of the D1-N87D samples were multiplied vertically as in Fig. 4 and were shifted vertically to coincide approximately at 2500 cm^{-1}.

Discussion

Both D1-N87A and D1-N87D *Synechocystis* sp. PCC 6803 cells exhibit photoautotrophic growth. The S-state cycling efficiency of the OEC can further be quantified by the miss parameter (α), which denotes the probability that the OEC fails to advance its oxidation state following a photochemical charge separation. The D1-N87A and wildtype PSII core complexes exhibit similar miss factors supporting their efficient S-state cycling. However, the miss factor for the D1-N87D PSII cores is twice that of the wildtype PSII cores. Further, the higher intensity of the first-flash bare-platinum electrode signal from D1-N87D PSII core complexes is indicative of damaged centers. Hence, the effect of D1-N87D mutation can be attributed to inefficient turnover or impairment in the stability of the OEC caused by perturbations in the hydrogen-bonding network. The observation that the D1-N87D, but not the D1-N87A, substitution impairs the S-state cycling illustrates that an Ala or Asn residue at D1 residue 87 is needed for efficient S-state cycling.

Fig. 1 shows the hydrogen-bonded network of water and amino acids around the D1-Asn^{87} residue in cyanobacterial PSII. We hypothesized that the change from D1-Asn^{87} in cyanobacteria to D1-A87 in spinach would perturb the hydrogen-bonded network around Water 1 (W1) and Water 2 (W2) bound to Mn4 in the OEC, thereby biasing the equilibrium distribution in the S_2 state toward the ($S = 5/2$) $g = 4.1$ EPR signal conformation. Hence, it was expected that, unlike wildtype cyanobacterial PSII, the S_2-state EPR spectra of D1-N87A PSII would exhibit an S_2-state $g = 4.1$ EPR signal resembling the S_2-state EPR spectrum of spinach PSII. However, the S_2-state EPR spectra of both D1-N87A and the D1-N87D PSII core complexes are similar to wildtype PSII, *i.e.* neither exhibits an S_2-state $g = 4.1$ EPR signal. These results may be reflective of subtle differences in the second-shell amino acid residues and hydrogen-bonded water molecules between spinach and cyanobacterial PSII that are not reflected in the primary amino acid sequences, which may favor the presence of the $g = 4.1$ EPR signal conformation in the S_2 state for spinach PSII. Further, differences in the extrinsic subunits between the two species may also contribute to the greater stability of the $S = 5/2$ conformation in spinach PSII relative to cyanobacterial PSII.

We next investigated whether D1-Asn^{87}–substituted PSII exhibits other properties like spinach PSII. Because it has been found that the oxygen-evolution activity of spinach PSII is more sensitive to Cl^- depletion than cyanobacterial PSII, the Cl^- effect on the steady-state oxygen-evolution activity of D1-N87A PSII and D1-N87D PSII was studied. Cl^- was depleted from the PSII core complexes by diffusion into a Cl^--

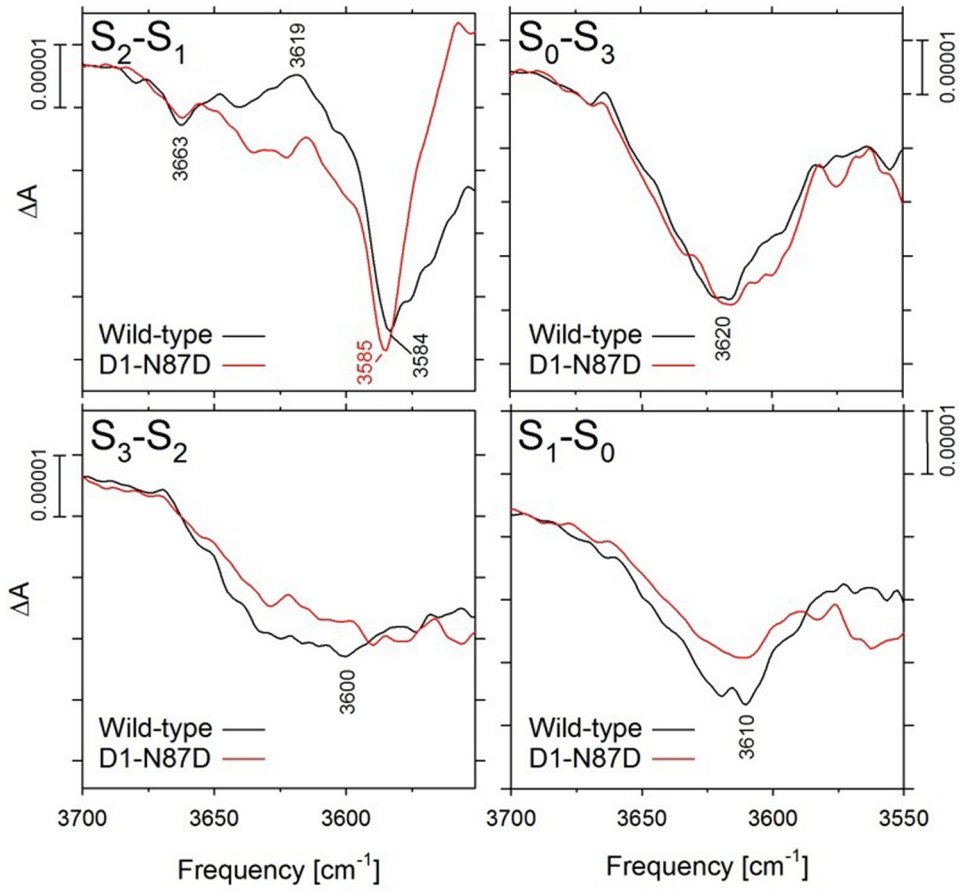

Figure 6. Comparison of the FTIR difference spectra of wildtype (*black*) and D1-N87D (*red*) *Synechocystis* PSII core complexes in the weakly hydrogen bonded O–H stretching region in response to four successive flash illuminations applied at 0 °C. The data were collected simultaneously with that shown in Fig. 4, were multiplied vertically as in Fig. 4, and were shifted vertically to coincide at ~3700 cm^{-1}. Note the different *vertical scales*.

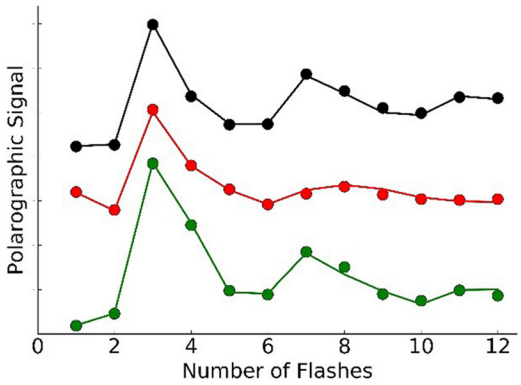

Figure 7. Comparison of flash oxygen-yield patterns of *Synechocystis* PSII core complexes from wildtype (*black*), D1-N87D (*red*), and D1-N87A (*green*). The data from wildtype and D1-N87D PSII are offset vertically for clarity.

Table 2
Kok-model fitting parameters for wildtype and D1-Asn^{87} substituted *Synechocystis* PSII core complexes
All S-state populations have a standard error of ±5%. The values represent averages of three or more samples.

	Misses, α	Double hits, β	S_0	S_1	S_2	S_3
	%	%	%	%	%	%
Wildtype	14 ± 1	3 ± 1	15	52	21	13
D1-N87D	29 ± 3	2 ± 1	6	64	14	16
D1-N87A	11 ± 3	5 ± 1	17	67	7	9

deficient medium. This technique has been previously used to remove Cl^- from spinach PSII; however, it has been found to be less effective for removal of Cl^- from cyanobacterial PSII, which has been attributed to a higher affinity of cyanobacterial PSII for Cl^- (3, 44–46). We find that Cl^- depletion affects the oxygen-evolution activity of D1-N87A PSII to a similar extent as spinach PSII. However, D1-N87D PSII exhibits a Cl^- effect like that of wildtype cyanobacterial PSII (3). This can be rationalized by the fact that a non-polar amino acid residue like alanine will affect the hydrogen-bonding network surrounding the OEC to a greater extent than a polar residue like aspartic acid. Hence, we conclude that D1 residue 87 plays an important role in the network of hydrogen-bonded waters and amino acid residues such that the effect of a single point mutation at D1 residue 87 can be translated to the Cl^--binding site ~13 Å away, as shown in Fig. 1. Further, the finding that the only statistically significant difference in the amino acid sequences of cyanobacterial and plant PSII around the OEC occurs at D1 residue 87 (2) can be correlated with the different Cl^--binding properties of PSII from the two species.

The water-filled hydrogen-bonded network of amino acids surrounding the OEC has been classified into several channels, namely the "back," "narrow," "large," and "broad" channels (47, 48). The broad channel includes Cl^-, D1-Asp^{61}, D2-Lys^{317}, D1-Glu^{65}, D1-Glu^{329}, and D1-Arg^{334} and has been assigned as the proton-exit pathway that facilitates the S_3 to S_0 transition. It

meets the narrow channel at D1-Asp^{61}, and this channel also connects to the O4 μ-oxo ligand of the OEC (49). Our finding that D1-Asn^{87}, a narrow-channel residue, modulates the Cl^--binding site indicates that the residues in the narrow channel modulate the functioning of the broad channel. Thus, there must be an extensive hydrogen-bonding network that interconnects the two channels.

To further probe the effects of the D1-Asn^{87} substitutions on the structure and hydrogen-bonding interactions around the OEC, FTIR characterization of D1-N87D and D1-N87A PSII was performed. The D1-N87D and D1-N87A substitutions alter amide and carboxylate vibrational modes throughout the mid-frequency regions of the S_{n+1}-*minus*-S_n FTIR difference spectra. Substitutions of other residues that participate in the networks of hydrogen bonds that surround the Mn_4CaO_5 cluster also cause numerous alterations in the mid-frequency regions of the S_{n+1}-*minus*-S_n FTIR difference spectra. Examples are D1-E65A (50), D1-Q165E (51), D1-N181A (13), D1-R334A (51), D2-E312A (50), and D2-K317A (3). In contrast, most substitutions of residues directly coordinated to the Mn_4CaO_5 cluster, *e.g.* D1-D170H (52), D1-E189Q or D1-E188R (54, 55), D1-E333Q (56), and D1-D342N (57), produce little or no changes to any of S_{n+1}-*minus*-S_n FTIR difference spectra. The changes to amide I, amide II, $\nu_{asym}(COO^-)$ and $\nu_{sym}(COO^-)$ modes in the S_{n+1}-*minus*-S_n spectra produced by the D1-N87D and D1-N87A substitutions are, therefore, consistent with the location of D1-Asn^{87} in the network of hydrogen bonds forming a water entry channel leading to the Mn_4CaO_5 cluster (58).

Features in the ν(C=O) regions of the S_{n+1}-*minus*-S_n FTIR difference spectra probe the extensive networks of hydrogen bonds surrounding the Mn_4CaO_5 cluster (50, 51, 59). The shifts of the features in this region, *e.g.* between 1748 and 1743 cm^{-1}, produced by the D1-N87D and D1-N87A substitutions are also consistent with D1-Asn^{87} participating in a network of hydrogen bonds that forms part of a water entry channel.

On the basis of quantum mechanics/molecular mechanics-based simulations (27), the broad positive feature observed between 3200 and 2500 cm^{-1} in the S_2-*minus*-S_1 spectrum has been assigned to the coupled O–H stretching vibrations of strongly hydrogen-bonded water molecules in a network that links D1-Asp^{61} with the Ca^{2+} ion and tyrosine Z (27). The feature is positive because the hydrogen bonds of the water molecules in this network are strengthened by the positive charge that develops on the Mn_4CaO_5 cluster during the S_1-to-S_2 transition (27). This feature is dominated by the O–H stretching vibrations of Water 1 (W1) and Water 2 (W2) bound to Mn4 in the OEC (27) and is eliminated by the D1-D61A mutation (26). The broad positive features in these regions of the S_3-*minus*-S_2, S_0-*minus*-S_3, and S_1-*minus*-S_0 spectra have been assigned to strongly hydrogen bonded O–H stretching vibrations of water molecules in networks of hydrogen bonds that are highly polarizable (28, 29). That the D1-N87D and D1-N87A mutations produce little change in these regions in any of the S_{n+1}-*minus*-S_n difference spectra implies that D1-Asn^{87} has limited influence on the strongly hydrogen-bonded water molecules that give rise to the broad features observed in these regions.

On the basis of quantum mechanics/molecular mechanics-based simulations (27), the features between 3700 and 3500 cm^{-1} in the S_2-*minus*-S_1 difference spectrum have been assigned to the coupled O–H stretching vibrations of weakly hydrogen-bonded water molecules in the network of hydrogen bonds that links D1-Asp^{61} with the Ca^{2+} ion and tyrosine Z (27). The features observed in the other S_{n+1}-*minus*-S_n spectra in this region are presumed to have the same origin (29, 38). Consequently, these features contain contributions from multiple water molecules. In the S_2-*minus*-S_1 spectra of D1-N87D and D1-N87A PSII core complexes, the positive feature at 3619 cm^{-1} was eliminated. In the S_3-*minus*-S_2 spectra, the intensity of the broad negative feature centered at 3600 cm^{-1} was diminished. These alterations are consistent with D1-Asn^{87} causing slight perturbations to this network.

In summary, our study provides new evidence on the function of the amino acid residue at D1 residue 87 in spinach and *Synechocystis* PSII. This residue helps in efficient S-state cycling of the OEC. The D1-N87A substitution in cyanobacteria, which replicates D1 residue 87 in spinach, alters the Cl^--binding properties such that D1-N87A PSII mimics spinach PSII. This indicates that D1 residue 87 modulates the effect of Cl^- on the PSII activity by perturbing the hydrogen-bonding network across the narrow and broad channels that interconnect D1 residue 87 with the Cl^--binding site.

Experimental procedures

Construction of mutant strains and extraction of PSII

The D1-N87A and D1-N87D mutations were constructed in the *psbA-2* gene of *Synechocystis* sp. PCC 6803 and transformed into a host strain of *Synechocystis* that lacks all three *psbA* genes and contains a hexahistidine tag fused to the C terminus of CP47. The control wildtype strain used in this study was constructed in identical fashion as the mutants, but with a transforming plasmid that carried no mutation (53). Single colonies were selected for their ability to grow on solid medium containing 5 μg/ml kanamycin monosulfate and 20 μg/ml gentamycin sulfate (53). D1-N87A cells were grown on solid BG-11 plates in the absence of glucose. The antibiotics were omitted from liquid cultures. The cells from small-scale liquid cultures were propagated in three 7-liter carboys as described previously (26) and bubbled with 1% CO_2 in air. The cells were grown with warm white fluorescent lighting at 28 °C (140 $\mu E\ m^{-2}\ s^{-1}$). The PSII extraction and purification were done under dim light conditions at 4 °C using a nickel-nitrilotriacetic acid super flow affinity resin (Qiagen) as described previously (60). The purified PSII core complexes were concentrated to ~1 mg of Chl/ml and stored in a buffer solution containing 1.2 M betaine, 10% (v/v) glycerol, 50 mM MES-NaOH (pH 6.0), 20 mM $CaCl_2$, 5 mM $MgCl_2$, 50 mM histidine, 1 mM EDTA, and 0.03% (w/v) *n*-dodecyl β-D-maltoside at −80 °C. Polymerase chain reaction amplification and sequencing of genomic DNA in the region of the *psbA* gene that contains the D1-Asn^{87} codon were performed on aliquots of each culture that were harvested to verify the integrity of the mutant cultures (53). No trace of the wildtype codon was detected in any of the mutant cultures. Spinach PSII membranes were prepared as described previously (61, 62) and suspended to

final chlorophyll concentrations of 5.0–7.0 mg ml^{-1} in 20 mM MES-NaOH (pH 6.0), 15 mM NaCl, and 30% (w/v) ethylene glycol.

Growth rate measurements

For measuring growth rates, wildtype, D1-N87A, and D1-N87D cells were grown photosynthetically in 100 ml of liquid BG-11 medium supplemented in the absence of glucose at 28 °C with a light intensity of 140 $\mu E\ m^{-2}\ s^{-1}$. Carbon dioxide was not bubbled at this stage. Growth was recorded by measuring the absorbance of the cultures at 730 nm using a Beckman DU-640 UV-visible spectrophotometer.

Analysis of amino acid residues

D1 sequences from Cyanobase and NCBI were compiled. For higher plants, 11 species were analyzed, all of which have Ala^{87}. For green algae, 59 species were analyzed of which 58 have Asn^{87} and 1 has Ala^{87}. For cyanobacteria, 94 sequences (some cyanobacteria have more than one D1 isoform) were analyzed, of which 81 have Asn^{87} and 13 have Ala^{87}.

Steady-state oxygen assay

PSII isolated from spinach, and wildtype, D1-N87A, and D1-N87D *Synechocystis* cells were stirred in low-chloride buffer ($[Cl^-]$ = 0.1 mM) in the dark for 2 min prior to each oxygen-evolution assay. The Cl^--dependent assays were performed by adding an appropriate volume of Cl^- from a stock solution in a buffer containing 1 M sucrose, 5 mM Ca^{2+} [using $Ca(OH)_2$], and MES (pH 6.5). Oxygen evolution was monitored with a Clark-type electrode, and the oxygen-assay chamber was maintained at 25 °C using a temperature-controlled water bath. The samples were illuminated with an Oriel 1000 W tungsten-halogen lamp. 250 μM 2-phenyl-1,4-benzoquinone with 1 mM K_3FeCN_6 was used as the electron acceptor, and 5 μg of Chl was used in each assay. The oxygen evolution of whole cells was carried out using a Clark electrode in the presence of 2 mM 2,6-dichloro-*p*-benzoquinone with 2 mM K_3FeCN_6 as electron acceptors (50).

EPR measurements

EPR samples of WT and D1-Asn^{87}–substituted *Synechocystis* PSII were prepared in 50 mM MES-NaOH (pH 6.5), 10% (v/v) glycerol, 1.2 M betaine, 20 mM $CaCl_2$, 5 mM $MgCl_2$, and 1 mM EDTA and were concentrated to 1 mg of Chl/ml using Amicon centrifugal cells having a 100-kDa cutoff. EPR samples of spinach PSII were prepared as described previously (9). The dark scan corresponding to the S_1 state was recorded. Then the S_2 state was generated by illuminating the sample with a red LED (623 nm) in a 200 K acetone/dry ice bath, and the S_2-state spectrum was recorded. The measurements were performed using a Bruker ELEXSYS E500 spectrometer equipped with a SHQ resonator and an Oxford ESR-900 continuous flow cryostat at 7.5 K. The EPR parameters used for recording the spectra are as follows: microwave frequency, 9.38 GHz; modulation frequency, 100 kHz; modulation amplitude, 19.95 G; microwave power, 5 milliwatt; sweep time, 84 s; conversion time, 41 ms; and time constant, 82 ms. Each spectrum is the average of two scans.

FTIR measurements

Purified PSII core complexes were exchanged into FTIR analysis buffer (40 mM sucrose, 10 mM MES-NaOH, pH 6.0, 5 mM $CaCl_2$, 5 mM NaCl, and 0.06% (w/v) *n*-dodecyl β-D-maltoside), concentrated to ~3.3 mg of Chl/ml, mixed with 1/10 volume of fresh 100 mM potassium ferricyanide (dissolved in water), spread to a diameter of ~13 mm in the center of a 25 × 2-mm diameter BaF_2 window, and dried lightly under a stream of dry nitrogen gas as described previously (26). Sample concentrations were adjusted so that the absolute absorbance of the amide I band at 1657 cm^{-1} was 0.7–1.1. To maintain the sample at 95% relative humidity in the FTIR sample compartment, six 1-μl droplets of a solution of 40% (v/v) glycerol in water were spotted around the periphery of the window, not touching the sample (29). Sealed samples were allowed to equilibrate at 0 °C in darkness in the FTIR sample compartment for 1.5 h, given 6 pre-flashes, and allowed to dark adapt for an additional 30 min (59). Mid-frequency FTIR spectra were recorded with a Bruker Vertex 70 spectrometer (Bruker Optics, Billerica, MA) as described previously (59).

After dark adaptation, six successive flashes were applied with an interval of 13 s between each. Two single-beam spectra were recorded before the first flash, and one single-beam spectrum was recorded starting 0.33 s after the first and subsequent flashes (each single-beam spectrum consisted of 100 scans). The 0.33-s delay was incorporated to allow for the oxidation of $Q_A^{\bullet-}$ by the ferricyanide. To obtain difference spectra corresponding to successive S-state transitions, the single-beam spectrum that was recorded after the n^{th} flash was divided by the single-beam spectrum that was recorded immediately before the n^{th} flash, and the ratio was converted to units of absorption. To estimate the background noise level, the second pre-flash single-beam spectrum was divided by the first, and the ratio was converted to units of absorption. The sample was dark-adapted for 30 min, and then the cycle was repeated. The cycle was repeated 15 times for each sample, and the difference spectra recorded with multiple samples were averaged.

Polarographic oxygen measurements

Flash-induced O_2 yields were measured polarographically using a bare platinum electrode with a silver counter electrode poised at −700 mV *versus* the normal hydrogen electrode. An EG&G xenon flash lamp controlled by an Arduino Uno (Ivrea, Italy) board provided periodic flashes interspersed by a delay time of 1 s. The measurements were performed in a buffer containing 1 M sucrose, 10 mM $CaCl_2$, 200 mM NaCl, and 50 mM MES-NaOH (pH 6.50) as described previously (3, 43). 2,6-Dichloro-*p*-benzoquinone and K_3FeCN_6 were also added to final concentrations of 500 μM and 1 mM, respectively, before taking measurements. The resulting period 4 oscillations were analytically fit to the VZAD model using the BOBYQA nonlinear optimization algorithm (42).

Author contributions—G. B, I. G., C. J. K., and R.J.D. performed experiments. G. B., I. G., C. J. K., R. J. D., and G. W. B. planned experiments, analyzed data, wrote the manuscript, and have given approval to the final version of the manuscript.

Acknowledgments—We thank Drs. Leslie Vogt and David Vinyard for discussions and helpful comments.

References

1. Suga, M., Akita, F., Hirata, K., Ueno, G., Murakami, H., Nakajima, Y., Shimizu, T., Yamashita, K., Yamamoto, M., Ago, H., and Shen, J. R. (2015) Native structure of photosystem II at 1.95 Å resolution viewed by femtosecond X-ray pulses. *Nature* **517,** 99–103 CrossRef Medline
2. Vogt, L., Vinyard, D. J., Khan, S., and Brudvig, G. W. (2015) Oxygen-evolving complex of photosystem II: an analysis of second-shell residues and hydrogen-bonding networks. *Curr. Opin. Chem. Biol.* **25,** 152–158 CrossRef Medline
3. Pokhrel, R., Service, R. J., Debus, R. J., and Brudvig, G. W. (2013) Mutation of lysine 317 in the D2 subunit of photosystem II alters chloride binding and proton transport. *Biochemistry* **52,** 4758–4773 CrossRef Medline
4. McEvoy, J. P., and Brudvig, G. W. (2006) Water-splitting chemistry of photosystem II. *Chem. Rev.* **106,** 4455–4483 CrossRef Medline
5. Kok, B., Forbush, B., and McGloin, M. (1970) Cooperation of charges in photosynthetic O_2 evolution-I: a linear four step mechanism. *Photochem. Photobiol.* **11,** 457–475 CrossRef Medline
6. Dismukes, G. C., and Siderer, Y. (1981) Intermediates of a polynuclear manganese center involved in photosynthetic oxidation of water. *Proc. Natl. Acad. Sci. U.S.A.* **78,** 274–278 CrossRef Medline
7. Haddy, A., Lakshmi, K. V., Brudvig, G. W., and Frank, H. A. (2004) Q-band EPR of the S_2 state of photosystem II confirms an S=5/2 origin of the X-band g=4.1 signal. *Biophys. J.* **87,** 2885–2896 CrossRef Medline
8. Pokhrel, R., and Brudvig, G. W. (2014) Oxygen-evolving complex of photosystem II: correlating structure with spectroscopy. *Phys. Chem. Chem. Phys* **16,** 11812–11821 CrossRef Medline
9. Vinyard, D. J., Khan, S., Askerka, M., Batista, V. S., and Brudvig, G. W. (2017) Energetics of the S_2 state spin isomers of the oxygen-evolving complex of photosystem II. *J. Phys. Chem. B* **121,** 1020–1025 CrossRef Medline
10. Ono, T., Zimmermann, J. L., Inoue, Y., and Rutherford, A. W. (1986) Electron paramagnetic resonance evidence for a modified S-state transition in chloride-depleted photosystem II. *Biochim. Biophys. Acta* **851,** 193–201 CrossRef
11. van Vliet, P., and Rutherford, A. W. (1996) Properties of the chloride-depleted oxygen-evolving complex of photosystem II studied by electron paramagnetic resonance. *Biochemistry* **35,** 1829–1839 CrossRef Medline
12. Boussac, A., Ishida, N., Sugiura, M., and Rappaport, F. (2012) Probing the role of chloride in photosystem II from *Thermosynechococcus elongatus* by exchanging chloride for iodide. *Biochim. Biophys. Acta* **1817,** 802–810 CrossRef Medline
13. Pokhrel, R., Debus, R. J., and Brudvig, G. W. (2015) Probing the effect of mutations of asparagine 181 in the D1 subunit of photosystem II. *Biochemistry* **54,** 1663–1672 CrossRef Medline
14. Lindberg, K., and Andréasson, L.-E. (1996) A one-site, two-state model for the binding of anions in photosystem II. *Biochemistry* **35,** 14259–14267 CrossRef Medline
15. Kühne, H., Szalai, V. A., and Brudvig, G. W. (1999) Competitive binding of acetate and chloride in photosystem II. *Biochemistry* **38,** 6604–6613 CrossRef Medline
16. Cooper, I. B., and Barry, B. A. (2008) Azide as a probe of proton transfer reactions in photosynthetic oxygen evolution. *Biophys. J.* **95,** 5843–5850 CrossRef Medline
17. Noguchi, T. (2013) Monitoring the reactions of photosynthetic water oxidation using infrared spectroscopy. *Biomed. Spectrosc. Imaging* **2,** 115–128 CrossRef
18. Chu, H.-A. (2013) Fourier transform infrared difference spectroscopy for studying the molecular mechanism of photosynthetic water oxidation. *Front. Plant Sci.* **4,** 146 Medline
19. Noguchi, T. (2008) Fourier transform infrared analysis of the photosynthetic oxygen-evolving center. *Coord. Chem. Rev.* **252,** 336–346 CrossRef
20. Noguchi, T. (2007) Light-induced FTIR difference spectroscopy as a powerful tool toward understanding the molecular mechanism of photosynthetic oxygen evolution. *Photosynth. Res.* **91,** 59–69 CrossRef Medline
21. Yamanari, T., Kimura, Y., Mizusawa, N., Ishii, A., and Ono T-a. (2004) Mid-to low-frequency Fourier transform infrared spectra of S-state cycle for photosynthetic water oxidation in *Synechocystis* sp. PCC 6803. *Biochemistry* **43,** 7479–7490 CrossRef Medline
22. Kimura, Y., Mizusawa, N., Ishii, A., Yamanari, T., and Ono T.-A. (2003) Changes of low-frequency vibrational modes induced by universal ^{15}N- and ^{13}C-isotope labeling in S_2/S_1 FTIR difference spectrum of oxygen-evolving complex. *Biochemistry* **42,** 13170–13177 CrossRef Medline
23. Noguchi, T., and Sugiura, M. (2003) Analysis of flash-induced FTIR difference spectra of the S-state cycle in the photosynthetic water-oxidizing complex by uniform ^{15}N and ^{13}C isotope labeling. *Biochemistry* **42,** 6035–6042 CrossRef Medline
24. Noguchi, T., Sugiura, M., Inoue, Y., Itoh, K., and Tasumi, M. (1999) FTIR studies on the amino-acid ligands of the photosynthetic oxygen-evolving Mn-cluster. In *Fourier Transform Spectroscopy: Twelfth International Conference*, pp. 459–460, Waseda University Press, Tokyo, Japan
25. Service, R. J., Yano, J., McConnell, I., Hwang, H. J., Niks, D., Hille, R., Wydrzynski, T., Burnap, R. L., Hillier, W., and Debus, R. J. (2011) Participation of glutamate-354 of the CP43 polypeptide in the ligation of manganese and the binding of substrate water in photosystem II. *Biochemistry* **50,** 63–81 CrossRef Medline
26. Debus, R. J. (2014) Evidence from FTIR difference spectroscopy that D1-Asp61 influences the water reactions of the oxygen-evolving Mn_4CaO_5 cluster of photosystem II. *Biochemistry* **53,** 2941–2955 CrossRef Medline
27. Nakamura, S., Ota, K., Shibuya, Y., and Noguchi, T. (2016) Role of a water network around the Mn_4CaO_5 cluster in photosynthetic water oxidation: a Fourier transform infrared spectroscopy and quantum mechanics/molecular mechanics calculation study. *Biochemistry* **55,** 597–607 CrossRef Medline
28. Noguchi, T., Suzuki, H., Tsuno, M., Sugiura, M., and Kato, C. (2012) Time-resolved infrared detection of the proton and protein dynamics during photosynthetic oxygen evolution. *Biochemistry* **51,** 3205–3214 CrossRef Medline
29. Noguchi, T., and Sugiura, M. (2002) FTIR detection of water reactions during the flash-induced S-state cycle of the photosynthetic water-oxidizing complex. *Biochemistry* **41,** 15706–15712 CrossRef Medline
30. Noguchi, T., and Sugiura, M. (2000) Structure of an active water molecule in the water-oxidizing complex of photosystem II as studied by FTIR spectroscopy. *Biochemistry* **39,** 10943–10949 CrossRef Medline
31. Noguchi, T., Inoue, Y., and Tang, X.-S. (1999) Structure of a histidine ligand in the photosynthetic oxygen-evolving complex as studied by light-induced Fourier transform infrared difference spectroscopy. *Biochemistry* **38,** 10187–10195 CrossRef Medline
32. Maréchal, A., and Rich, P. R. (2011) Water molecule reorganization in cytochrome *c* oxidase revealed by FTIR spectroscopy. *Proc. Natl. Acad. Sci. U.S.A.* **108,** 8634–8638 CrossRef Medline
33. Hou, L.-H., Wu, C.-M., Huang, H.-H., and Chu, H.-A. (2011) Effects of ammonia on the structure of the oxygen-evolving complex in photosystem II as revealed by light-induced FTIR difference spectroscopy. *Biochemistry* **50,** 9248–9254 CrossRef Medline
34. Freier, E., Wolf, S., and Gerwert, K. (2011) Proton transfer via a transient linear water-molecule chain in a membrane protein. *Proc. Natl. Acad. Sci. U.S.A.* **108,** 11435–11439 CrossRef Medline
35. Shimada, Y., Suzuki, H., Tsuchiya, T., Tomo, T., Noguchi, T., and Mimuro, M. (2009) Effect of a single-amino acid substitution of the 43 kDa chlorophyll protein on the oxygen-evolving reaction of the cyanobacterium *Synechocystis* sp. PCC 6803: analysis of the Glu354Gln mutation. *Biochemistry* **48,** 6095–6103 CrossRef Medline
36. Iwata, T., Paddock, M. L., Okamura, M. Y., and Kandori, H. (2009) Identification of FTIR bands due to internal water molecules around the quinone binding sites in the reaction center from *Rhodobacter sphaeroides*. *Biochemistry* **48,** 1220–1229 CrossRef Medline
37. Suzuki, H., Sugiura, M., and Noguchi, T. (2008) Monitoring water reactions during the S-state cycle of the photosynthetic water-oxidizing center: detection of the DOD bending vibrations by means of Fourier transform infrared spectroscopy. *Biochemistry* **47,** 11024–11030 CrossRef Medline
38. Noguchi, T. (2008) FTIR detection of water reactions in the oxygen-evolving centre of photosystem II. *Philos. Trans. R. Soc. Lond. B Biol. Sci* **363,** 1189–1195 CrossRef Medline

39. Garczarek, F., and Gerwert, K. (2006) Functional waters in intraprotein proton transfer monitored by FTIR difference spectroscopy. *Nature* **439,** 109–112 CrossRef Medline
40. Kandori, H., and Shichida, Y. (2000) Direct observation of the bridged water stretching vibrations inside a protein. *J. Am. Chem. Soc.* **122,** 11745–11746 CrossRef
41. Kandori, H. (2000) Role of internal water molecules in bacteriorhodopsin. *Biochim. Biophys. Acta* **1460,** 177–191 CrossRef Medline
42. Vinyard, D. J., Zachary, C. E., Ananyev, G., and Dismukes, G. C. (2013) Thermodynamically accurate modeling of the catalytic cycle of photosynthetic oxygen evolution: a mathematical solution to asymmetric Markov chains. *Biochim. Biophys. Acta* **1827,** 861–868 CrossRef Medline
43. Vinyard, D. J., and Brudvig, G. W. (2015) Insights into substrate binding to the oxygen-evolving complex of photosystem II from ammonia inhibition studies. *Biochemistry* **54,** 622–628 CrossRef Medline
44. Sandusky, P., and Yocum, C. (1986) The chloride requirement for photosynthetic oxygen evolution: factors affecting nucleophilic displacement of chloride from the oxygen-evolving complex. *Biochim. Biophys. Acta* **849,** 85–93 CrossRef
45. Sandusky, P. O., and Yocum, C. F. (1984) The chloride requirement for photosynthetic oxygen evolution: analysis of the effects of chloride and other anions on amine inhibition of the oxygen-evolving complex. *Biochim. Biophys. Acta* **766,** 603–611 CrossRef
46. Lindberg, K., Vänngård, T., and Andréasson, L.-E. (1993) Studies of the slowly exchanging chloride in photosystem II of higher plants. *Photosynth. Res.* **38,** 401–408 CrossRef Medline
47. Ho, F. M., and Styring, S. (2008) Access channels and methanol binding site to the $CaMn_4$ cluster in photosystem II based on solvent accessibility simulations, with implications for substrate water access. *Biochim. Biophys. Acta* **1777,** 140–153 CrossRef Medline
48. Linke, K., and Ho, F. M. (2014) Water in photosystem II: structural, functional and mechanistic considerations. *Biochim. Biophys. Acta* **1837,** 14–32 CrossRef Medline
49. Vassiliev, S., Zaraiskaya, T., and Bruce, D. (2012) Exploring the energetics of water permeation in photosystem II by multiple steered molecular dynamics simulations. *Biochim. Biophys. Acta* **1817,** 1671–1678 CrossRef Medline
50. Service, R. J., Hillier, W., and Debus, R. J. (2010) Evidence from FTIR difference spectroscopy of an extensive network of hydrogen bonds near the oxygen-evolving Mn_4Ca cluster of photosystem II involving D1-Glu65, D2-Glu312, and D1-Glu329. *Biochemistry* **49,** 6655–6669 CrossRef Medline
51. Service, R. J., Hillier, W., and Debus, R. J. (2014) Network of hydrogen bonds near the oxygen-evolving Mn_4CaO_5 cluster of photosystem II probed with FTIR difference spectroscopy. *Biochemistry* **53,** 1001–1017 CrossRef Medline
52. Debus, R. J., Strickler, M. A., Walker, L. M., and Hillier, W. (2005) No evidence from FTIR difference spectroscopy that aspartate-170 of the D1 polypeptide ligates a manganese ion that undergoes oxidation during the S_0 to S_1, S_1 to S_2, or S_2 to S_3 transitions in photosystem II. *Biochemistry* **44,** 1367–1374 CrossRef Medline
53. Debus, R. J., Campbell, K. A., Gregor, W., Li, Z.-L., Burnap, R. L., and Britt, R. D. (2001) Does histidine 332 of the D1 polypeptide ligate the manganese cluster in photosystem II?: an electron spin echo envelope modulation study. *Biochemistry* **40,** 3690–3699 CrossRef Medline
54. Strickler, M. A., Hillier, W., and Debus, R. J. (2006) No evidence from FTIR difference spectroscopy that glutamate-189 of the D1 polypeptide ligates a Mn ion that undergoes oxidation during the S_0 to S_1, S_1 to S_2, or S_2 to S_3 transitions in photosystem II. *Biochemistry* **45,** 8801–8811 CrossRef Medline
55. Kimura, Y., Mizusawa, N., Ishii, A., Nakazawa, S., and Ono T.-A. (2005) Changes in structural and functional properties of oxygen-evolving complex induced by replacement of D1-glutamate 189 with glutamine in photosystem II. *J. Biol. Chem.* **280,** 37895–37900 CrossRef Medline
56. Service, R. J., Yano, J., Dilbeck, P. L., Burnap, R. L., Hillier, W., and Debus, R. J. (2013) Participation of glutamate-333 of the D1 polypeptide in the ligation of the Mn_4CaO_5 cluster in photosystem II. *Biochemistry* **52,** 8452–8464 CrossRef Medline
57. Strickler, M. A., Walker, L. M., Hillier, W., Britt, R. D., and Debus, R. J. (2007) No evidence from FTIR difference spectroscopy that aspartate-342 of the D1 polypeptide ligates a Mn ion that undergoes oxidation during the S_0 to S_1, S_1 to S_2, or S_2 to S_3 transitions in photosystem II. *Biochemistry* **46,** 3151–3160 CrossRef Medline
58. Retegan, M., and Pantazis, D. A. (2016) Interaction of methanol with the oxygen-evolving complex: atomistic models, channel identification, species dependence, and mechanistic implications. *Chem. Sci.* **7,** 6463–6476 CrossRef Medline
59. Debus, R. J. (2015) FTIR studies of metal ligands, networks of hydrogen bonds, and water molecules near the active site Mn_4CaO_5 cluster in photosystem II. *Biochim. Biophys. Acta* **1847,** 19–34 CrossRef Medline
60. Strickler, M. A., Walker, L. M., Hillier, W., and Debus, R. J. (2005) Evidence from biosynthetically incorporated strontium and FTIR difference spectroscopy that the C-terminus of the D1 polypeptide of photosystem II does not ligate calcium. *Biochemistry* **44,** 8571–8577 CrossRef Medline
61. Berthold, D. A., Babcock, G. T., and Yocum, C. F. (1981) A highly resolved, oxygen-evolving photosystem II preparation from spinach thylakoid membranes: EPR and electron-transport properties. *FEBS Lett.* **134,** 231–234 CrossRef
62. Beck, W. F., de Paula, J. C., and Brudvig, G. W. (1985) Active and resting states of the oxygen-evolving complex of photosystem II. *Biochemistry* **24,** 3035–3043 CrossRef Medline